Characteristics of non-tectonic tremors around the Lützow-Holm Bay, East Antarctica, during 2013–2015

Characteristics of non-tectonic tremors around the Lützow-Holm Bay, East Antarctica, during 2013–2015

Yuya Tanaka[a], Yoshihiro Hiramatsu[b,*], Yoshiaki Ishihara[c,1], Masaki Kanao[d]

[a]Graduate School of Natural Science and Technology, Kanazawa University
Kakuma, Kanazawa, Ishikawa, 920-1192, Japan

[b]School of Natural System, College of Science and Engineering, Kanazawa University
Kakuma, Kanazawa, Ishikawa, 920-1192, Japan

[c]Japan Aerospace Exploration Agency
Yoshinodai 3-1-1, Chuo-ku, Sagamihara, Kanagawa, 252-5210, Japan

[1]Current affiliation: National Institute for Environmental Studies, 16-2, Onogawa, Tsukuba, Ibaraki 305-8506, Japan.

[d]National Institute of Polar Research, Research Organization of Information and Systems
10-3, Midori-cho, Tachikawa, Tokyo, 190-8518, Japan

[*]Corresponding author. E-mail address: yoshizo@staff.kanazawa-u.ac.jp (Yoshihiro Hiramatsu)

Other authors' e-mail address: mail2ytanaka@gmail.com (Yuya Tanaka), ishihara.yoshiaki@nies.go.jp (Yoshiaki Ishihara), kanao@nipr.ac.jp (Masaki Kanao)

Abstract

Characteristics of non-tectonic tremors, excited mainly by the interaction within the cryosphere, were investigated using seismic waveform data of 2013–2015 recorded at broadband stations on the east coast of the Lützow-Holm Bay (LHB), East Antarctica. The tremors were classified into three types by spectral and waveform features. Type A events have long durations, typically several hours to days, with high amplitudes of spectra over 1–8 Hz. They occur dominantly in austral summers. Type B events have characteristically irregular variations in discrete dominant frequencies in spectra. Type C events are harmonic tremors with discrete dominant frequencies in spectra that vary regularly with time. Type B and C events show similar seasonal variations: they are numerous around April and less so in austral winter. Comparison of spectra between seismic waves and infrasound, together with satellite images, suggests that type A events originated from storm-induced swells near off-LHB. Source locations of type C events and satellite images suggest that type C events are likely to result from the collision/crevassing of ice blocks in fast-sea-ice in LHB. Similar seasonal variations of type B and C events imply that these two events have similar origins.

Keywords:

cryosphere; fast-sea-ice; harmonic tremor; microbaroms; MODIS

1. Introduction

Non-tectonic tremors and quakes, which are excited by physical interactions among the atmosphere, oceans, cryosphere, and the surface of the solid Earth, have often been observed in polar regions (e.g., Kanao et al., 2012; MacAyeal et al., 2008, 2009; Nettles and Ekström, 2010; Peng et al., 2014). Some tremors are caused by ice-related phenomena such as collision of sea-ice, opening and closing of oceanic tide cracks, collapse of icebergs, and the movements of glaciers and ice sheets. Moreover, ice-related phenomena are useful as a proxy to assess climate change in polar regions. Ekström et al. (2006) found clear seasonal variation of the occurrence of glacier earthquakes in Greenland, with the greatest number in summer, and increase of their annual number, reflecting a change in climate conditions in the Arctic. In this regard, the monitoring of ice quakes and tremors is important to elucidate the long-term variation of the surface environment in polar regions.

Along the eastern coast of Lützow-Holm Bay (LHB) in East Antarctica, seismic observations with broadband seismographs have been conducted at Syowa Station (SYO; 69.0°S, 39.6°E) and near the outcrop field sites. Non-tectonic tremors and quakes have been recorded around LHB. Kanao et al. (2012) reported a tremor with harmonic overtones in 1997 winter that might be related to a sea-ice discharge event, which were imaged clearly by the National Oceanic and Atmospheric Administration (NOAA) satellite. Kanao et al. (2012) also reported microseisms in the frequency range of 0.05–1 Hz at SYO and their weakened amplitude in austral winter. Expansion of the sea-ice spreading area and the increase of their thickness depressed the oceanic swell energy recorded at SYO seismograms. It is particularly interesting that they also pointed out some non-tectonic signals with frequencies higher than 1 Hz, implying that these signals are of local surface origin, presumably associated with ice-related phenomena.

Recently, Kanao et al. (2017) reported ice-related tremors around LHB, particularly in April 2015, by checking the power spectral density (PSD) of short-period and broadband seismograms at SYO. Comparison with Moderate Resolution Imaging Spectroradiometer (MODIS) imagery and tremor activities suggested that the tremors occurred along large cracks inside the fast-sea-ice, between offshore icebergs and the edge of the fast-sea-ice, between the fragmented fast-sea-ice and packed-sea-ice, or other origins. Nevertheless, the tremors source locations have not been identifiable from seismic waveform data alone. Furthermore, Kanao et al. (2017) focused only on the harmonic tremors and causes of other tremors, which we describe later, has not been specified.

Another tool to monitor the surface environment in polar regions is infrasound. Infrasound observations have continued since 2008 at SYO (Ishihara et al., 2009). Ishihara et al. (2015) analyzed infrasound waves recorded at SYO in 2008–2010. They demonstrated that the amplitude of microbaroms became low during austral winters and inferred that a larger amount of sea-ice, distributed around the LHB, decreased ocean wave loading effects. Murayama et al. (2017) presented information related to the source locations of tremors in April 2015. By analyzing infrasound waveforms recorded at two tripartite arrays on the east coast of LHB during the same period as that examined by Kanao et al. (2017), they located infrasound sources of which frequencies were higher than 1 Hz. Most of the infrasound sources were located within the sea-ice area in LHB. The MODIS imagery implied that these sources corresponded to locations near the fragmentation of icebergs and within the packed-sea-ice areas. However, the consistency between infrasound observations and seismic observations has not been examined. If we locate a tremor source and compare it to the infrasound sources, then we may obtain the information which link the two sources.

This study, through consideration of the recently conducted studies described above, specifically examines non-tectonic tremors with frequencies higher than 1 Hz recorded at seismic stations around LHB during a longer period of three years: 2013–2015. The identified tremors were classified into several types based on spectral and waveform features. We discuss those seasonal variations and their origins together with the characteristic features of infrasound waveforms and spectra, source locations of two nontectonic-tremors estimated from seismograms, and MODIS imagery. Through the discussion, we suggest the causes of not only harmonic tremors but also other non-tectonic tremors and a possible link between the tremor source and the infrasound source.

2. Data and Method

2.1. Seismic waveform data

Seismic observations have been conducted since 1959 at SYO using a short-period seismometer with a natural period of 1.0 s (Eto, 1962). A three-component broadband seismometer of STS–1 has been operating since 1989 at SYO (Fig. 1; Nagasaka et al., 1992). Since 1997, a three-component broadband seismometer of Güralp CMG–40T has also been installed at field outcrop stations, i.e. Langhovde, Skallen, and Rundvagshetta (Fig. 1). We use velocity waveform data recorded by STS–1 at SYO and CMG–40T at the other three stations. The sampling frequencies of STS–1 and CMG–40T are 20 Hz and 100 Hz, respectively. The analysis period extends from January 2013 through December 2015.

2.2. Identification of tremors

This study specifically examines tremors with frequency higher than 1 Hz, of which P-waves and S-waves are not clear and the duration is longer than 5 min, to distinguish tremors from short-duration ice quakes. To enhance the detectability of tremors, we applied a band-pass filter of 2–8 Hz to velocity waveforms.

We identified the nontectonic-tremors by visual inspection of velocity waveforms and its spectrograms calculated from velocity waveforms using fast Fourier transform (FFT). The start time of the tremor was set to the time when the amplitude exceeds the noise level and the end time was set to the time when the amplitude becomes below the noise level. In making spectrograms, we set the time window length as 60 s for FFT and shifted it to every 30 s. The noise levels of N–S component is usually ~5 percent smaller than that of E–W component and ~30 percent smaller than that of U–D component, resulting ~30% higher signal-to-noise ratio of N–S component than the other two components. Furthermore, continuous meteorological and infrasound observations have been conducted at SYO, allowing us to compare seismic observation to those observations. We, thus, mainly used velocity waveforms and spectrograms of N–S component at SYO for visual inspection.

2.3. Locating of sources of nontectonic-tremors

Tremors observed in this study show unclear onset, making it impossible to locate those sources using a conventional hypocenter determination procedure. For tectonic tremors, a cross-correlation function of envelope waveforms at close stations is available to estimate the travel time differences of major phases, enabling us to locate those sources (e.g., Obara, 2002). In this study, the distance between the stations is so large that the coherency between the observed waveforms at different stations is usually low. Plausible reasons of low coherency could be a relatively wide range of the azimuth and a radiation pattern of tremors. A waveform could be different between stations with different azimuths by reflecting the radiation pattern. Also, for small tremors which might occur in the relatively close area to SYO, we could not observe the waveform at all stations. However, for some large tremors, we found a coherent part in envelope waveforms at all stations. Therefore, we were able to estimate travel time differences of large nontectonic-tremors recorded at different stations as follows.

First, we calculated envelope waveforms from root-mean-square amplitudes of velocity waveforms of the N–S component of each station with a moving time window of 300 s. Second, the cross-correlation function of envelope waveforms was calculated for each pair of the stations by selecting a proper time window, which was selected by trial and error. We used the lag time, which gives the maximum value of the cross-correlation function, as a travel time difference of a pair of the stations. In this study, we obtained lag times of six pairs from four stations for each event. Third, we estimated the hypocenters of nontectonic-tremors with grid search using the lag times. For the grid search, we set a tentative hypocenter at every 0.1° × 0.1° on the surface in the area shown in the upper-right panel of Fig. 4 and calculated the theoretical travel time between a tentative hypocenter and a station. We assumed a velocity of 1500 m/s by referring acoustic velocity of sound in water (Carmona et al., 2015) and Rayleigh wave velocity in ice (Tsoflias et al., 2008). As the optimal hypocenter, we chose a grid at which the sum of squares of the residuals (Res^2) between the observed and the theoretical travel time differences at the stations (τ_i and t_i, respectively), defined by $Res^2 = \sum_{i=1}^{6} |\tau_i - t_i|^2$, reaches the minimum. We also estimated the 95% confidence area of the hypocenter based on the chi-square distribution.

3. Results and Discussion

3.1. Classification of tremors

After identifying 84 tremors in 2013, 148 in 2014, and 198 in 2015, we classified the tremors into three types (type A–C) based on waveform and spectrogram characteristics (Fig. 2). Type A tremors, nontectonic-tremors with an extremely long duration (several hours to days), are shown by the spectrogram to be excited at frequencies of 1–8 Hz. Type B are nontectonic-tremors characterized by an irregular (nonlinear featured) variation in a dominant frequency with time. The dominant frequency components of type B events are discrete. Type C, typical harmonic tremors, show a continuous shift, an increase or decrease (gliding-up or down), of dominant frequencies with time. In addition, they show clear overtones. We identified 79 type A events, 200 type B events, and 151 type C events in 2013–2015.

3.2. Seasonal variation in nontectonic-tremors

We show the monthly number and the monthly cumulative duration of the tremors for each type in Fig. 3. Variations both in number and in cumulative duration are somewhat different between these types. For type A, the number is the smallest among the three types, although the duration is the longest. Seasonal variations in those are similar each year, large in February–April, austral summer, and small around August, austral winter (Fig. 3 upper panels). For type B, the total number in three years is the largest. The seasonal variations show an almost identical pattern each other, large around April, austral summer, and small in May–November, austral winter (Fig. 3 middle panels).

Both the variations are the largest in 2015, although the variation in monthly mean temperature at SYO is almost identical in each year. Therefore, we consider that the variation in the number is related not to a local climate change but to a condition change of fast-sea-ice, such as crevassing and discharging, in LHB (e.g., Kanao et al., 2017). Type C events were fewer in 2013, but more numerous in 2014 and 2015 (Fig. 3 lower panels). This increase is similar to that observed for type B. The seasonal variations of type C events are not clear for 2013 because of the small number of the events, whereas those are apparently similar to those of type B in 2014 and 2015. The similarities and differences in the variations suggest that the cause of type A events differs from those of type B and C events, although type B and C events might have a common cause.

3.3. Source location of type C tremors

Applying the procedure described in sub-section 3.2, we tried to estimate the source locations of type C events in 2015, because Murayama et al. (2017) reported ice–related infrasound around LHB and we can compare our results to their results. As a result, we estimated the source locations of two type C events on 1 and 5 April 2015 (Fig. 4). Both sources are located within or the edge of fast-sea-ice in LHB, although the 95%

confidence area is large because of the limited and orientated distribution of seismic stations along the eastern coast of LHB. Fig. 5 depicts MODIS imagery around LHB obtained on 24 March, and 11 and 17 April in 2015. These images show clearly that the two type C events are closely related to a change in the condition of the fast-sea-ice in LHB. We can recognize obviously that the development of a break off as well as a movement (enlargement of sea area near by the fast-sea-ice shown as a black area) of the fast-sea-ice in LHB from on late March to middle April in 2015 (Fig. 5). It is noteworthy that the estimated source locations correspond to areas where the break off and/or the movement of the fast-sea-ice was observed. Kanao et al. (2017) reported that a large volume of the fast-sea-ice was discharged in the northwestern part of LHB on early April in 2015, which might be related to the occurrence of nontectonic-tremors. Murayama et al. (2017) estimated the source locations of ice quakes from array analyses of infrasound data recorded at sites along the eastern coast of LHB in April 2015. The source locations of ice quakes (infrasound sources) are concentrated in the northwestern part of LHB. The results of these two studies are coincident with our estimations of the source locations of the two type C events.

3.4. Causes of nontectonic-tremors

For non-tectonic tremors of all types, the number presents seasonal variation in each year: active in austral summers and calm in austral winters. A possible cause of this seasonality is a seasonal variation in weather conditions and resulting cryosphere conditions around LHB. Infrasound observations have been conducted since 2008 at SYO (Ishihara et al., 2015). Infrasound signals include the background oceanic signals, termed as microbaroms in a frequency range of 0.1–0.3 Hz. Stormy weather, such as a blizzard, enhances ocean waves and oceanic-originated microbaroms. Therefore, we compare seismic data to infrasound data as a proxy of ocean wave conditions. Fig. 6 portrays examples of spectrograms of seismic waves which include two type A events, the sum of the velocity amplitude spectrum (VAS) of seismic waves over a range of 1–8 Hz and that of power spectrum density (PSD) of microbaroms over a range of 0.1–0.3 Hz (Ishihara et al., 2015), both of which were observed at SYO, in austral summer (left panels) and winter (right panels) seasons. We do not use PSD of seismic waves for comparison of the sums because the similarity is most distinct between VAS of seismic waves and PSD of microbaroms. During the occurrence of type A events in the austral summer, we recognize clearly that the temporal variations of the sum of VAS and that of PSD are very similar (Fig. 6 left upper-middle and left lower-middle panels). A large

PSD, together with a long duration up to several days, of microbaroms indicates the occurrence of a blizzard around LHB. This fact suggests that type A events have a common origin with microbaroms. In other words, the type A events are possibly originated from strong ocean waves in stormy weather: storm-induced swells. However, during the austral winter, we can recognize no coherent power of seismic waves with that of microbaroms, although the PSD of microbaroms is large (Fig. 6 right upper-middle and right lower-middle panels). In other words, no type A event is observed in spite of strong ocean waves in stormy weather. A large difference can be found in the ice condition around LHB between the two seasons from MODIS imagery. In the austral summer, fast-sea-ice in LHB is fragile; no sea-ice is distributed off the edge of fast-sea-ice (Fig. 6 lower left panel). However, in the austral winter, fast-sea-ice is well developed in LHB. Large fields of packed sea-ice are distributed off the edge of fast-sea-ice (Fig. 6 lower right panel). The former strengthens the occurrence of tremors in close areas to the stations than the latter because the source location of microbaroms could be farther (offshore into the southern Indian Ocean) for the latter than for the former. The same phenomena were reported for microseism in the 1–20 s period band recorded at seismic stations in Antarctica by Grob et al. (2011). They reported that the growth of sea-ice in austral winter can impede microseism generation near coastal areas.

In fact, the amplitude of VAS of a microseism band, 0.05–1 Hz, is large when type A events occur in the austral summer, but it is low when no type A event occurs in the austral winter (Fig. 6). This finding suggests that the type A events might originate from storm-induced swells.

Harmonic nontectonic-tremors such as type C events are observed widely in polar regions: around the Ross Sea (MacAyeal et al., 2009), the marginal sea of the Antarctic Peninsula (Bohnenstiehl et al., 2005; Dziak et al., 2009), and the continental margin of Dronning Maud Land (Eckstaller et al., 2006; Muller and Eckstaller, 2003). The spectral features of type C events, which are high-frequency harmonic tremors with frequencies higher than 1 Hz, are the same as those reported in previous works, suggesting that type C events are caused by the collision and rubbing of ice blocks. As discussed in Kanao (2017), the activity of harmonic tremors recorded at seismic stations in LHB is apparently related closely to a breaking-off of fast-sea-ice or discharge events in LHB. In this study, the sources of type C events are located within or the edge of the fast-sea-ice in LHB. This evidence is the first directly showing that harmonic tremors occur around the fast-sea-ice area. Furthermore, the MODIS imagery shows that the source locations are close to a break-off area of fast-sea-ice in LHB, as described in sub-section 3.3 (Fig. 4). Therefore, we conclude from this evidence that breaking-off and calving of fast-sea-ice and the collision of ice blocks are causes of type C events. Kanao et al. (2017) reported that harmonic tremors occurred independently from weather conditions. The difference in seasonal variation in the monthly number and the monthly cumulative duration between the type A and the type C events can be interpreted by the type A events from storm-induced swells and type C events from breaking and collision of ice blocks.

For the type B event, we have no direct information related to the source location. The seasonal variations in the number and the cumulative duration of the type B events are similar to those of the type C events rather than the type A events (Fig. 3). Furthermore, the spectral feature of the type B events, i.e. discrete (nonlinear) dominant frequencies, is similar to that of type C events rather than the type A events (Fig. 2). These similarities suggest that the cause of the type B events might resemble the cause of type C. Therefore, we consider that the type B events also might be related to the breaking-off and calving of fast-sea-ice and the collision of ice blocks in LHB. Their nonlinear features in type B suggest less rigid origins such as crashing phenomena between the packed-sea-ice and fragmentation of fast-sea-ice in and around the bay.

4. Conclusions

We investigated non-tectonic tremors during 2013–2015 recorded at broadband seismic stations around LHB, East Antarctica. Features of waveforms and velocity amplitude spectra enable us to classify the tremors into three types: A–C types. Type A events are characterized by a long duration and a wide spectrum strength over 1–8 Hz. Type B and C events are characterized by discrete dominant frequencies in the spectrum. They show, respectively, irregular and a regular variation in the dominant frequencies with time. In other words, type C events are harmonic tremors. We also examine seasonal variations in the monthly number and cumulative duration of each type. All types show clear seasonal variation, but with patterns that differ between the types. The occurrence of type A events concentrates during February–April in austral summer. Type B and C events tend to occur around April and less in May–November. Comparison of the strength of spectra between seismic waves and infrasound shows clearly that type A events are closely related to the strength of microbaroms in austral summer, but show no relation in austral winter. The MODIS imagery reveals a difference of the development of fast-sea-ice and packed sea-ice in/around LHB, suggesting that well-developed fast-sea-ice/packed sea-ice prevent observation of tremors generated near coastal areas. Therefore, we infer that type A events originated from storm-induced swells. The sources of two type C events are estimated to be located in and around fast-sea-ice in LHB. They show consistency with the breaking-off of fast-ice observed from the MODIS imagery. These facts, together with information from previous studies, suggest that type C events are likely to result from the breaking and collision of ice blocks. Similarities between type B and C events imply that the cause of the type B events is common to that of type C events rather than to that of type A events.

References

Bohnenstiehl, D., Dziak, R.P., Parlk, M., Matsumoto, H., 2005. Seismicity of the Polar Seas: The potential for hydroacoustic monitoring of tectonic and volcanic processes. The 12th Seoul International Symposium on Polar Science, Ansan, 17–19 May 2005, 11–14.

Carmona, E., Almendros, J., Alguacil, G., Soto, I.J., Luzon, F., Ibanez, J.M., 2015. Identification of T-waves in the Alboran Sea. Geophys. 172, 3179–3188. doi 10.1007/s00024-014-1018-1.

Dziak, R.P., Parlk, M., Lee, W.S., Matsumoto, H., Bohnenstiehl, D.R., Haxel, J.H., 2009. Tectonomagmatic activity and ice dynamics in the Bransfield Strait back-arc basin, Antarctica. In: the 16th Inter. Sympos. on Polar Sci.; 10–12 June 2009; Incheon. Incheon: KOPRI; pp. 59–68.

Eckstaller, A., Müller, C., Ceranna, L., Hartmann, G., 2006. The geophysics observatory at Neumayer Stations (GvN and NM-II) Antarctica, Polarforschung, 76, 3–24.

Ekstrom, G., Nettles, M., Tsai, V.C., 2006. Seasonality and increasing frequency of Greenland glacial earthquakes. Science 311. doi:10.1126/science.1122112.

Eto, T., 1962. On the electromagnetic seismographs at Syowa Base, Antarctica. Nankyoku Shiryô (Antarct. Rec.), 14, 1168–1170. (in Japanese with English abstract)

Grob, M., Maggi, A., Stutzmann, E., 2011. Observations of the seasonality of the Antarctic microseismic signal, and its association to sea ice variability. Geophysical

Research Letters 38, L11302. http://dx.doi.org/10.1029/2011GL047525.

Ishihara, Y., Kanao, M., Yamamoto, M.-Y., Toda, S., Matsushima, T., Murayama, T., 2015. Infrasound observations at Syowa Station, East Antarctica: implications for detecting the surface environmental variations in the polar regions. Geoscience Frontiers 6, 285–296.

Ishihara, Y., Yamamoto, M.-Y., Kanao, M., 2009. Current status of infrasound pilot observation at Japanese Islands and SYOWA Antarctica, and development of new infrasound sensor using optical sensing method. AGU Fall Meeting, San Francisco, California, USA, A13D-0244.

Kanao, M., Maggi, A., Ishihara, Y., Yamamoto, M.-Y., Nawa, K., Yamada, A., Wilson, T., Himeno, T., Toyokuni, G., Tsuboi, S., Tono, Y., Anderson, K., 2012. Seismic wave interactions between the atmosphere–ocean–cryosphere and geosphere in polar regions. In: Kanao, M., Takenaka, H., Murai, Y., Matsushima, J., Toyokuni, G. (Eds.), Seismic Waves–Research and Analysis, ISBN 978-953-307-944-8, InTech, Rijeka, Croatia, 1–20.

Kanao, M., Murayama, T., Yamamoto, M.-Y, Ishihara, Y., 2017. Seismic tremors and their relation to cryosphere dynamics in April 2015 around the Lützow-Holm Bay. East Antarctica. International Journal of Geosciences 8, 1025–1047. https://doi.org/10.4236/ijg.2017.88058.

MacAyeal, R.D., Okal, E.A., Aster, R.C., Bassis, N.J., 2008. Seismic and hydroacoustic tremor generated by colliding icebergs. Journal of Geophysical Research 113, F03011. doi:10.1029/2008 JF001005.

MacAyeal, D.R., Okal, E.A., Aster, R.C., Bassis, J.N., 2009. Seismic observations of glaciogenic ocean waves on icebergs and ice shelves. Journal of Glaciology 55, 193–206. https://doi.org/10.3189/002214309788608679.

Muller, C., Eckstaller, A., 2003. Local seismicity detected by the Neumayer seismological network, Dronning Maud Land, Antarctica: Tectonic earthquakes and ice-related seismic phenomena. IX International Symposium on Antarctic Earth Science Program and Abstracts, Potsdam, p. 236.

Murayama, T., Kanao, M., Yamamoto, M.-Y, Ishihara, Y., Matsushima, T., Kakinami, Y., Okada, K., Miyamachi, H., Nakamoto, M., Takeuchi, Y., Toda, S., 2017. Time–space variations in infrasound sources related to environmental dynamics around Lützow–Holm Bay, east Antarctica. Polar Science 14, 39–48.

Nagasaka, K., Kaminuma, K., Shibuya, K., 1992. Seismological observations by a three-component broadband digital seismograph at Syowa Station, Antarctica. Recent Progress in Antarctic Earth Science, ed. by Y. Yoshida *et al.* Tokyo, Terra Sci. Publ., 595–601. (TERRAPUB e-Library) http://www.terrapub.co.jp/e-library/aes/pdf/RP0595.PDF.

Nettles, M., Ekström, G., 2010. Glacial earthquakes in Greenland and Antarctica. The Annual Review of Earth and Planetary Sciences 38, 467–491. https://doi.org/10.1146/annurev-earth-040809-152414.

Obara, K., 2002. Nonvolcanic deep tremor associated with subduction in southwest Japan. Science 296, 1679–1681.

Peng, Z., Walter, J.I., Aster, R.C., Nyblade, A., Wiens, D.A., Anandakrishnan, S., 2014. Antarctic icequakes triggered by the 2010 Maule Earthquake in Chile. Nature Geoscience 7, 677–681. https://doi.org/10.1038/ngeo2212.

Tsoflias, G.P., Ivanov, J., Anandakrishnan, S., Miller, R., 2008. Use of active source seismic waves in glaciology. Symposium on the Application of Geophysics to Engineering and Environmental Problems 1240–1243. https://doi.org/10.4133/1.2963234.

Acknowledgements

We are grateful to the many people who have collaborated with seismic/infrasound observation around LHB, especially for members of the Japanese Antarctic Research Expeditions (JARE). We also thank for two anonymous reviewers for constructive comments. This work was supported by JSPS KAKENHI Grant Number 26241010 (PI Masaki Kanao). We used the MODIS imagery from National Aeronautics and Space Administration (NASA). We also used temperature data from Japan Meteorological Agency. The authors declare that they have no competing interests related to the

contents of this work.

Figure captions

Fig. 1. Locations of seismic stations around the Lützow-Holm Bay (LHB) used for this study.

Fig. 2. Examples of velocity seismograms and velocity amplitude spectra of the N–S component recorded at SYO: (upper) type A, (middle) type B, and (lower) type C tremors.

Fig. 3. Temporal variations in (left row) monthly number and (right row) monthly cumulative duration of (upper) type A, (middle) type B, and (lower) type C events. The dashed line in each panel shows the monthly mean temperature at SYO.

Fig. 4. Results of the source locating of two type C events, (a) on 1 April 2015 and (b) on 5 April 2015. (upper-left) Examples of a waveform and a spectrogram at SYO. (upper-right) A red star shows the source location of an event. The area enclosed by a

dashed line is the 95% confidence area of the source location and blue triangles are the seismic stations used for the source locating. The background image is the MODIS imagery on 11 April 2015. (lower left) Envelope waveforms of N–S component velocity waveforms at each station. Red lines show a time window for calculation of cross correlation function (lower-right) cross correlation functions of envelope waveforms at two stations.

Fig. 5. MODIS imagery on (upper) 24 March, (middle) 11 April, and (lower) 17 April in 2015. Blue lines represent the break off within the fast-sea-ice. Red stars and the dashed lines are the same as those in Fig. 4.

Fig. 6. Comparison between (upper) velocity amplitude spectrum (VAS) of N–S component velocity waveform at SYO, (upper middle) the sum of VAS over a frequency range of 1–8 Hz, (lower middle) the sum of power spectrum density (PSD) of microbaroms over a frequency range of 0.1–0.3 Hz recorded at SYO. Lower panels are MODIS imagery (left) on 16 February 2014 (in austral summer) and (right) 23 September 2014 (in austral winter). The left panels include two type A events and the right panels no events. The amplitude for seismic wave in austral winter is

approximately one order smaller than that in austral summer.

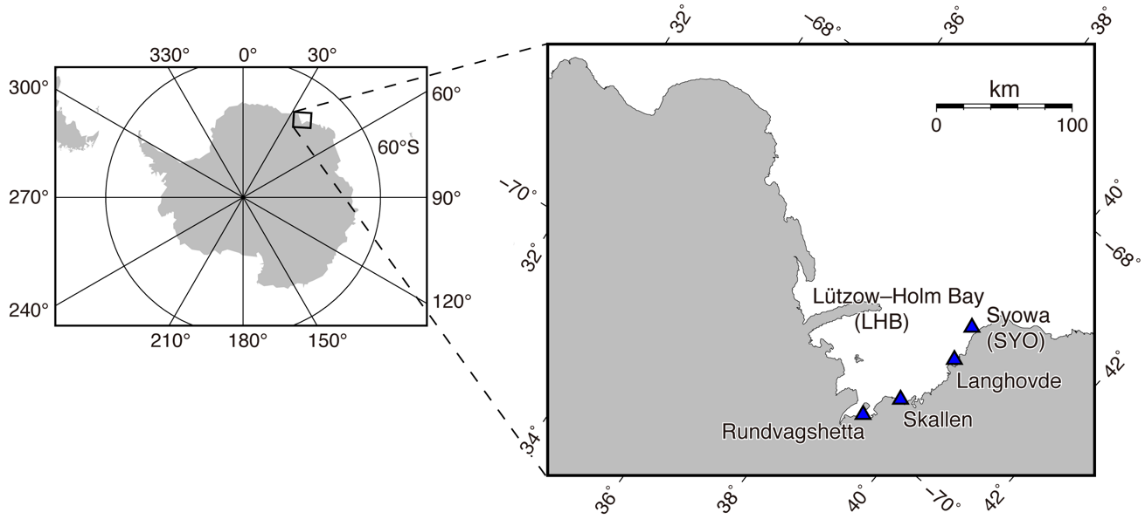
330°
0°
30°
300°
60°
60°S
270°
90°
240°
120°
210°
180°
150°
km
0
100
Lützow–Holm Bay
(LHB)
Syowa
(SYO)
Langhovde
Skallen
Rundvagshetta

Figure 1.

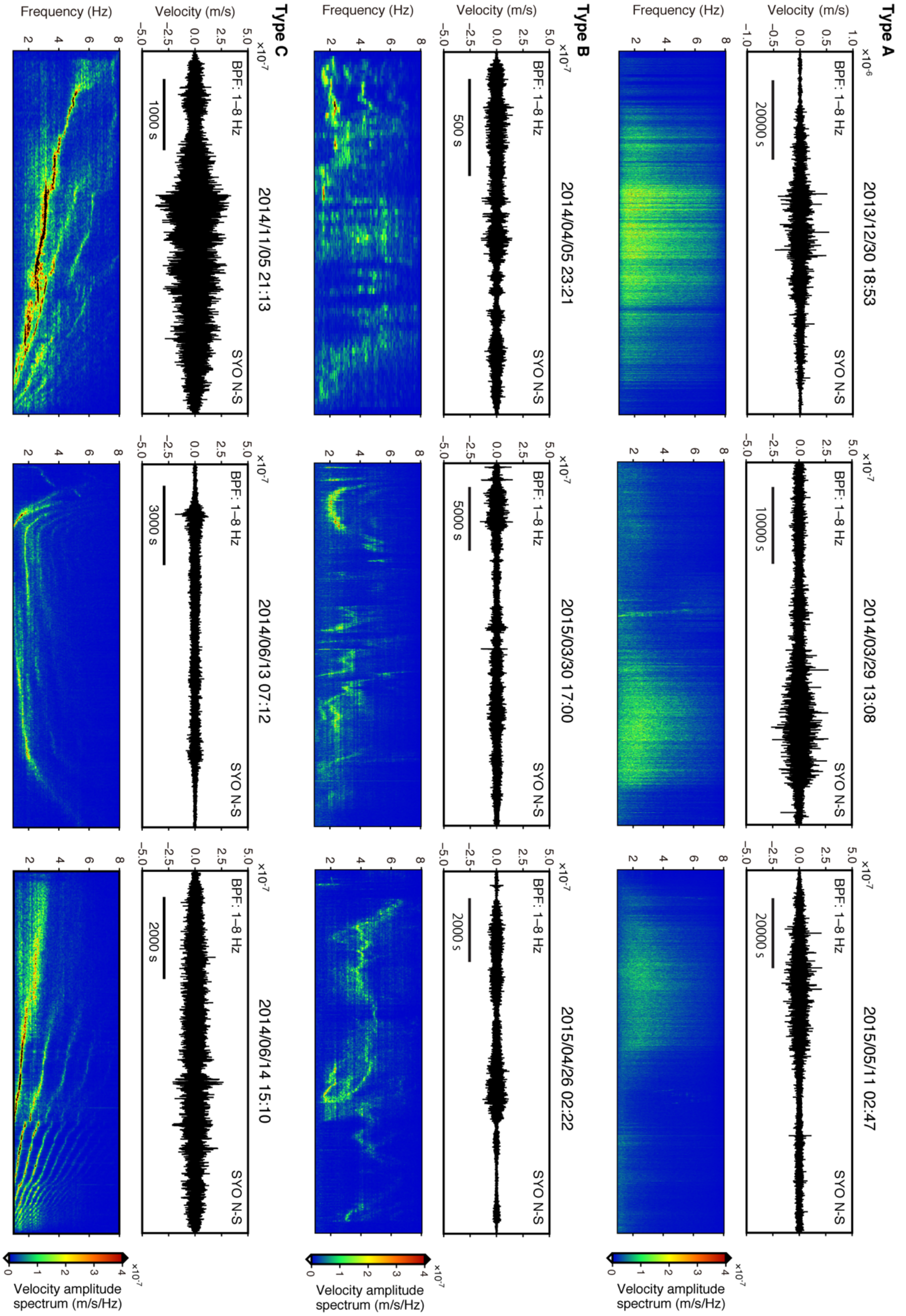
Type A
2013/12/30 18:53
2014/03/29 13:08
2015/05/11 02:47
Type B
2014/04/05 23:21
2015/03/30 17:00
2015/04/26 02:22
Type C
2014/11/05 21:13
2014/06/13 07:12
2014/06/14 15:10
BPF: 1–8 Hz
SYO N-S
Velocity (m/s)
Frequency (Hz)
20000 s
10000 s
500 s
5000 s
2000 s
1000 s
3000 s
Velocity amplitude spectrum (m/s/Hz)

Figure 2.

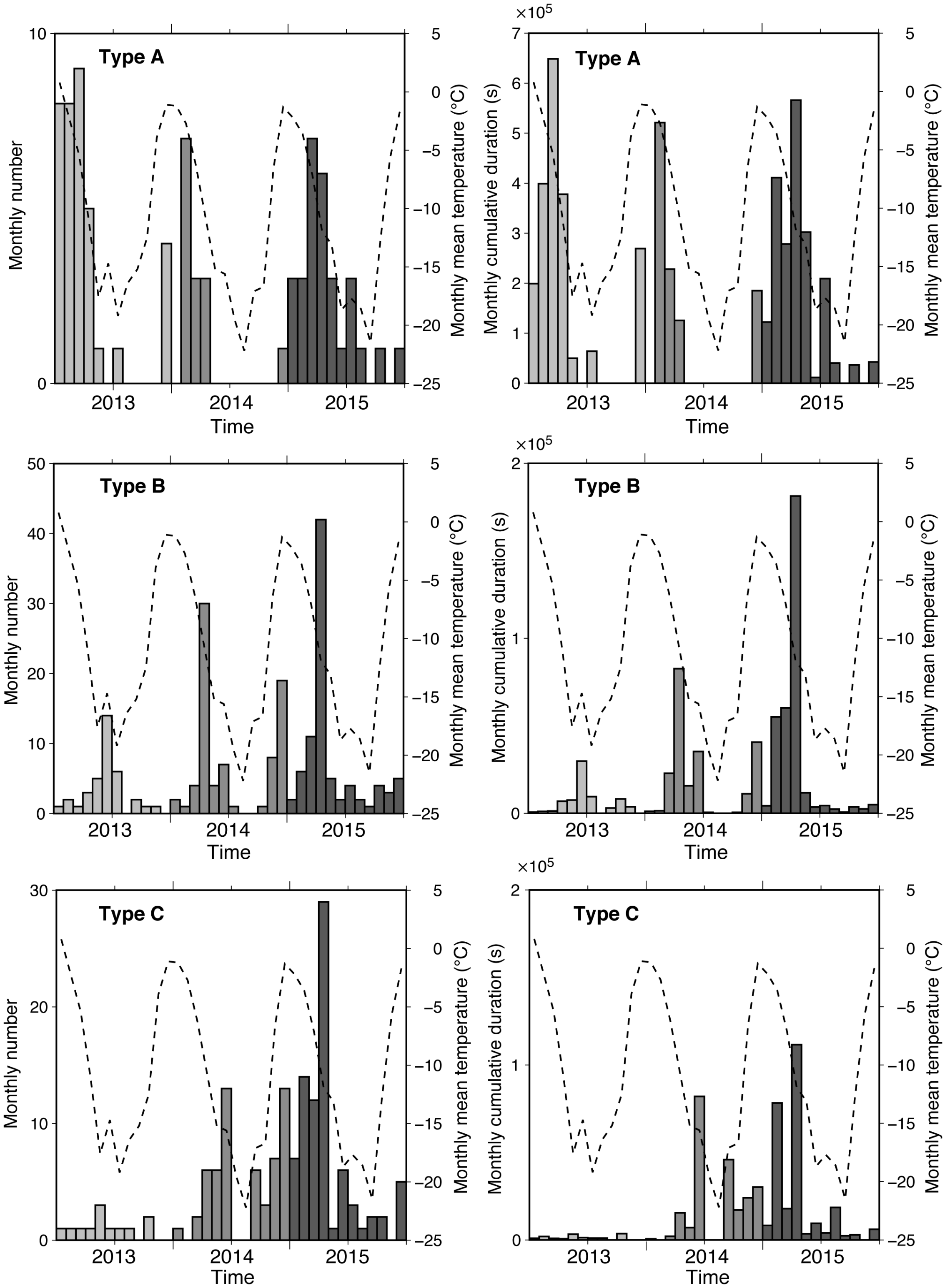
Type A
Type B
Type C
Monthly number
Monthly cumulative duration (s)
Monthly mean temperature (°C)
×10^5
2013
2014
2015
Time

Figure 3.

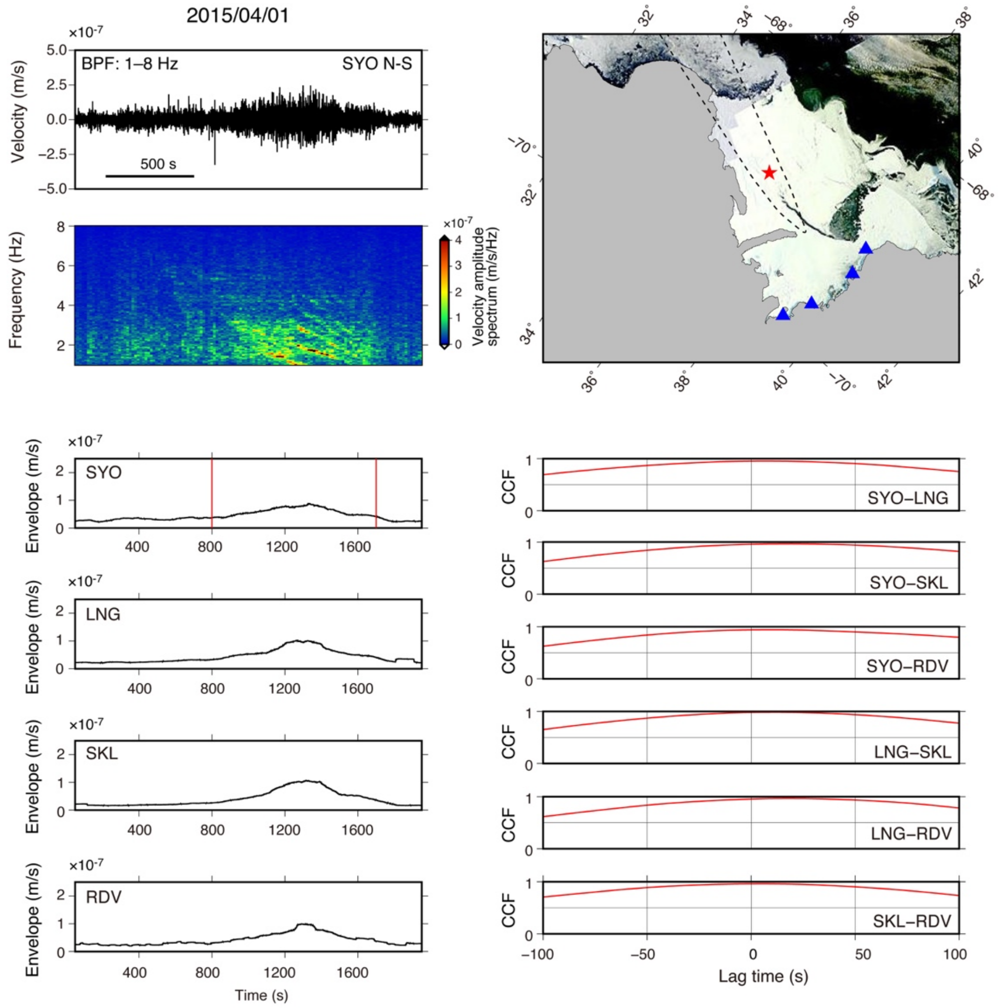
2015/04/01
BPF: 1–8 Hz
SYO N-S
Velocity (m/s)
500 s
Frequency (Hz)
Velocity amplitude spectrum (m/s/Hz)
SYO
LNG
SKL
RDV
Envelope (m/s)
Time (s)
SYO–LNG
SYO–SKL
SYO–RDV
LNG–SKL
LNG–RDV
SKL–RDV
CCF
Lag time (s)

Figure 4a

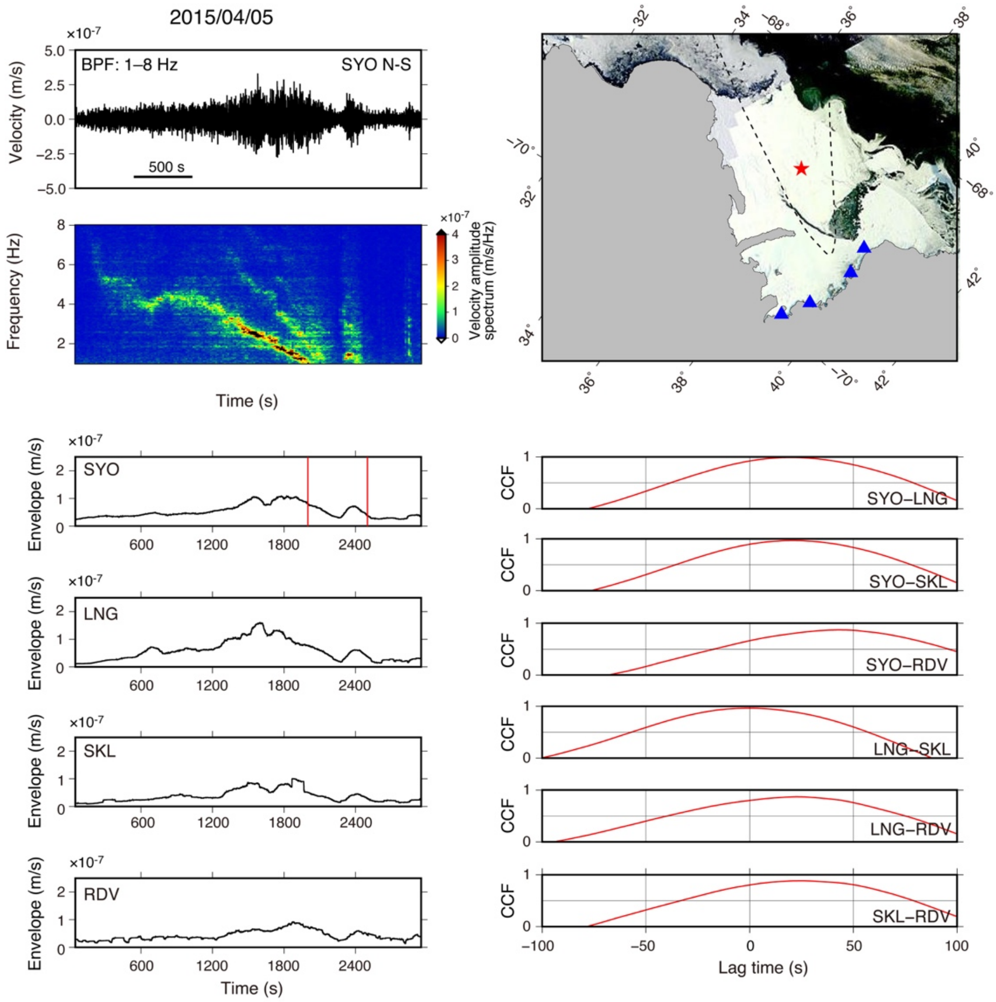
2015/04/05
BPF: 1–8 Hz
SYO N-S
Velocity (m/s)
500 s
Frequency (Hz)
Velocity amplitude spectrum (m/s/Hz)
Time (s)
Envelope (m/s)
SYO
LNG
SKL
RDV
CCF
SYO–LNG
SYO–SKL
SYO–RDV
LNG–SKL
LNG–RDV
SKL–RDV
Lag time (s)

Figure 4b.

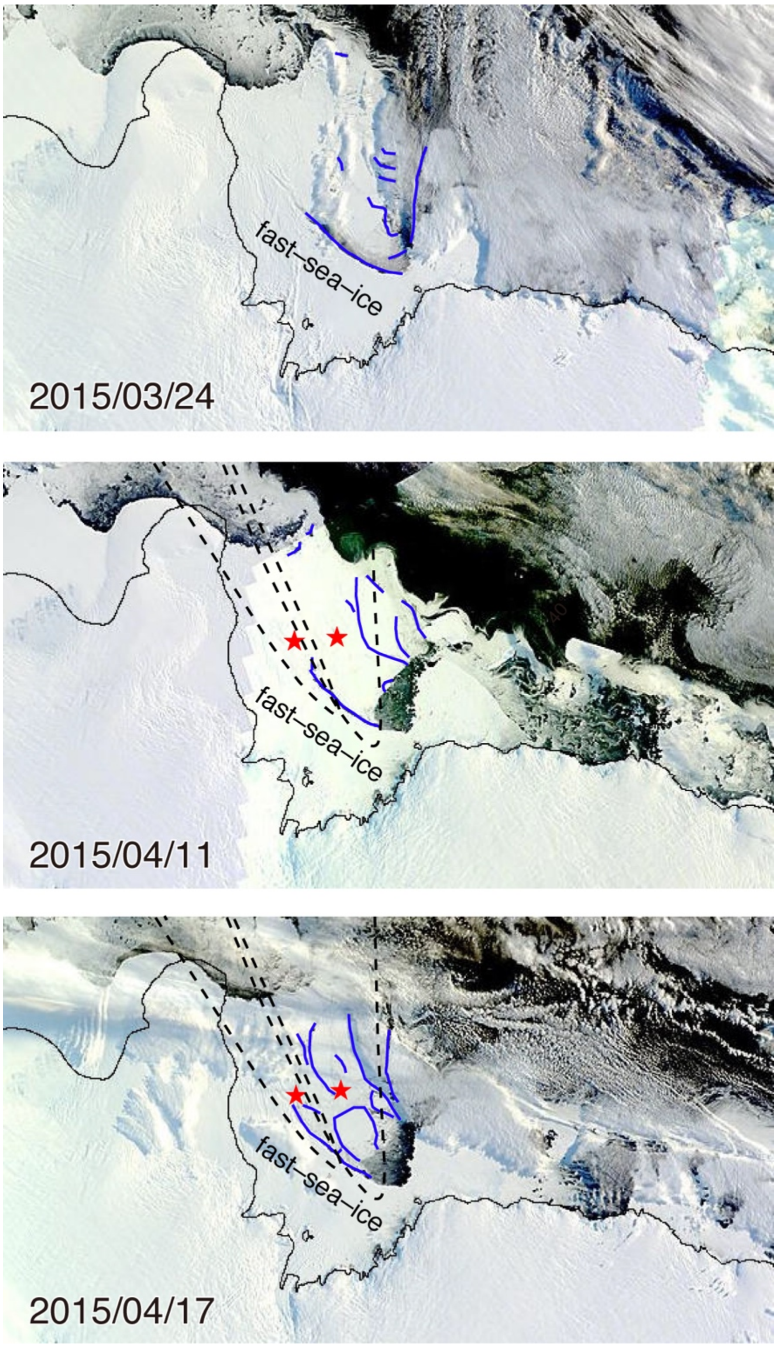
fast–sea–ice
2015/03/24
fast–sea–ice
2015/04/11
fast–sea–ice
2015/04/17

Figure 5.

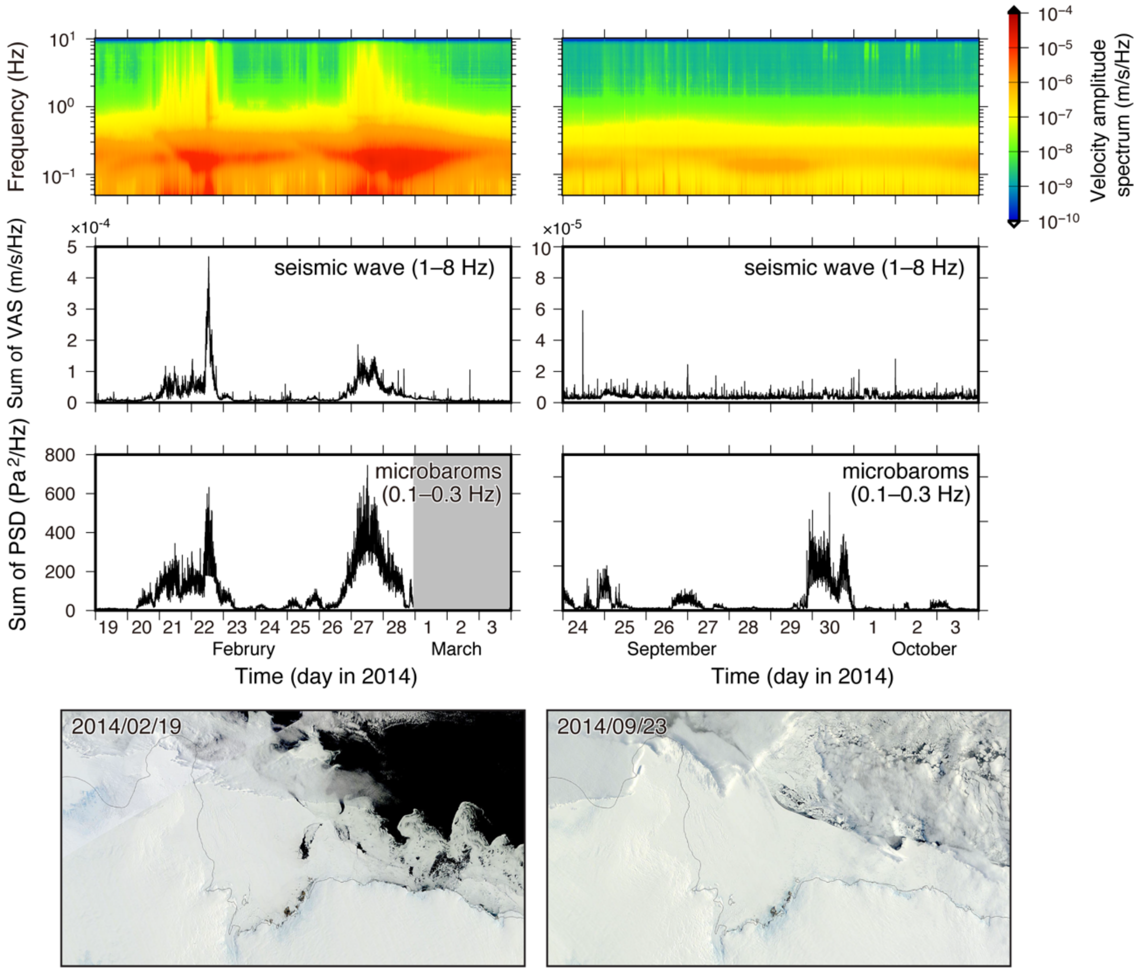

Frequency (Hz)
Velocity amplitude spectrum (m/s/Hz)
Sum of VAS (m/s/Hz)
×10-4
×10-5
seismic wave (1–8 Hz)
seismic wave (1–8 Hz)
Sum of PSD (Pa 2/Hz)
microbaroms (0.1–0.3 Hz)
microbaroms (0.1–0.3 Hz)
Februry
March
September
October
Time (day in 2014)
Time (day in 2014)
2014/02/19
2014/09/23

Figure 6.